JOURNAL OF MATERIALS SCIENCE 23 (1988) 1419–1424

Long-range ordering of vacancies in bcc α-AlFeSi

PING LIU, G. L. DUNLOP
Department of Physics, Chalmers University of Technology, S-41296 Göteborg, Sweden

Long-range ordering of iron vacancies in the bcc α-AlFeSi intermetallic compound has been investigated by a combination of selected-area electron diffraction, convergent beam electron diffraction, energy dispersive X-ray spectroscopy and high resolution lattice imaging. The superstructure was found to be rhombohedral with a space group $R\bar{3}$ and lattice parameters $a_{sup} = 3.076$ nm, $c_{sup} = 3.263$ nm. A model for the superstructure is presented and it is shown that the model is in agreement with experimental observations.

1. Introduction

Intermetallic phases containing aluminium, iron and silicon are very common in aluminium alloys because iron and silicon are usually present as substantial impurity elements. The intermetallic bcc α-AlFeSi phase, $Im\bar{3}$ $a = 1.256$ nm, [1] often precipitates during solidification or heat treatment of aluminium alloys [2]. This phase is probably not an equilibrium phase but it is thought to be stabilized by the presence of transition metal elements such as manganese or chromium which can dissolve in its structure [3].

While the basic structure of α-AlFeSi is bcc, extra reflections have been found in selected-area electron diffraction (SAED) patterns in some investigations [4–6]. These observations have led to suggestions that the phase can exhibit long-range ordering under certain conditions. Explanations for the extra reflections have been previously given in terms of either a hexagonal superstructure [5] or a new phase (α_T-AlFeSi) with a monoclinic crystal structure [6]. However, neither of these proposed structures agree with systematically tilted SAED patterns or with the diffuse electron scattering which can be observed in certain beam directions [7].

In the present work the superstructure for ordered α-AlFeSi has been determined using many of the functions available in a modern analytical microscope, i.e. SAED, convergent beam electron diffraction (CBED), energy dispersive X-ray spectroscopy (EDX), and high resolution imaging.

2. Experimental details

Precipitates of bcc α-AlFeSi, which exhibited extra reflections in SAED were found in the directionally chill cast dilute Al–Fe–Si alloys (A, B and C) whose compositions are given in Table I. Details concerning the preparation, solidification and heat treatment of these alloys have been given elsewhere [4]. Additional precipitates of α-AlFeSi, which did not exhibit extra reflections in SAED, were also investigated. These precipitates were found in a die-cast Al–9Si–3Cu (wt %) alloy.

Thin foils for transmission electron microscopy were prepared by jet electropolishing 3 mm discs in an electrolyte consisting of 25% HNO_3 in methanol at 30 V and −30° C. The die-cast Al–Si–Cu alloy was electropolished in an electrolyte of 20% HNO_3 and 2% NH_4OH in methanol at 30 V and room temperature. The thin foils were examined in a Jeol-2000FX scanning transmission electron microscope (TEM/STEM) equipped with a Link Systems-860 EDX spectrometer. Analyses by EDX were quantified using the Link Systems RTS 2/FLS computer program, which applies the thin foil approximation with experimental K_{XSi} values, uses stored standard spectra of pure elements and corrects for absorption [8]. Specimen thickness measurements used in the absorption correction were obtained by the convergent beam technique [9]. Photographic densities (blackening) of SAED patterns were measured using a Kontron IBAS interactive image analysis system.

TABLE I Compositions (wt %) of the Al–Fe–Si alloys investigated

Alloy	Fe	Si	Impurities	Al
A	0.51	0.13	0.04	bal.
B	0.28	0.13	0.04	bal.
C	0.27	0.13	0.004	bal.

3. Results

Two different morphologies of bcc α-AlFeSi which were found in alloys A, B and C are shown in Fig. 1. Both of these morphologies gave extra reflections in SAED patterns while precipitates of this phase found in the Al–Si–Cu alloy did not give extra reflections. SAED patterns with $[1\,1\,0]_{bcc}$ zone axes are shown for both situations in Fig. 2. Extra reflections at 1/3 $(\bar{1}\,1\,2)_{bcc}$ and 1/3 $(2\,\bar{2}\,2)_{bcc}$ can be seen in Fig. 2a while these reflections are absent in Fig 2b.

A CBED pattern corresponding to the SAED pattern in Fig. 2a (i.e. $[1\,1\,0]_{bcc}$ zone axis) is shown in Fig. 3. This pattern contains a ring from a higher order Laue zone (HOLZ). The spacing of reciprocal planes parallel to the electron beam can be calculated by use of the geometric relationship between

0022–2461/88 $03.00 + .12

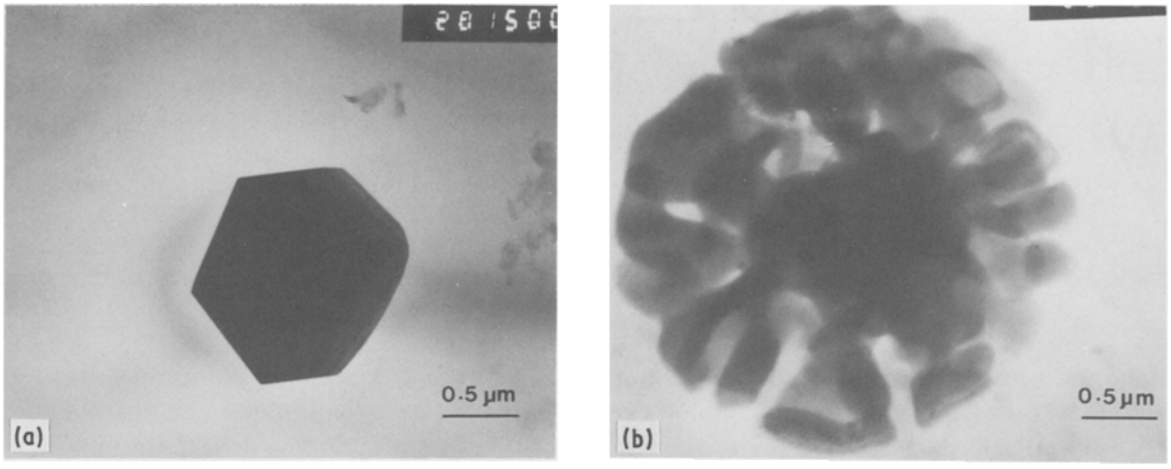

Figure 1 Two common morphologies of bcc α-AlFeSi observed in alloys A, B and C (TEM).

the radius of HOLZ rings and crystallographic parameters [10–12]

$$d^*_{uvw} = G^2 \frac{\lambda}{2} \quad (1)$$

where d^*_{uvw} is the spacing of reciprocal lattice planes in the direction $[u\,v\,w]_{bcc}$, G is the radius of the HOLZ ring and λ is the wavelength of electrons. The camera length was calibrated using known reflections in the zero order Laue zone (HOLZ) and measurements of the radius of the HOLZ ring gave, using Equation 1

$$d^*_{uvw} = 1/1.7763\,\text{nm}^{-1} \quad (2)$$

This is the same as d^*_{110} for bcc α-AlFeSi, i.e.

$$d^*_{110} = 1/r_{110} = 1/1.7763\,\text{nm}^{-1} \quad (3)$$

where r_{110} is the length of the crystal lattice direction vector [1 1 0] for bcc α-AlFeSi. Use of this information to solve the SAED pattern in Fig. 2a shows that the extra reflections may be due to a superlattice having an orthorhombic structure with the following lattice parameters

$$a^* = 1/3(\bar{1}\,1\,2)_{bcc} \quad b^* = 1/3(2\,\bar{2}\,2)_{bcc} \quad c^* = (1\,1\,0)_{bcc}$$

$$a_{sup} = 1.538\,\text{nm} \quad b_{sup} = 1.088\,\text{nm} \quad c_{sup} = 0.888\,\text{nm}$$

However, careful examination of the symmetry of the CBED pattern in Fig. 3 shows that the whole pattern symmetry is 1. Therefore, the superlattice cannot be orthorhombic [13] and this solution is incorrect.

A $\langle 1\,1\,1\rangle_{bcc}$ zone axis CBED pattern from the same crystal as in Figs 2a and 3 is shown in Fig. 4a together with an SAED pattern with the same zone axis. Strong reflections in the SAED pattern come from the bcc primary lattice while the weaker reflections at 1/3 $\{1\,1\,2\}_{bcc}$ are due to the superlattice. For comparison, CBED and SAED patterns from the same $\langle 1\,1\,1\rangle_{bcc}$ zone axis for disordered α-AlFeSi are shown in Fig. 4b. It can readily be seen that the CBED pattern for the ordered structure has two more HOLZ rings than that for the disordered α-AlFeSi. Measurements of the radii of these extra HOLZ rings and use of Equation 1 show that the ordered structure has an interplanar spacing in reciprocal space which is one-third of that for the disordered structure in the $\langle 1\,1\,1\rangle_{bcc}$.

The CBED pattern for the ordered structure in Fig. 4a has a whole pattern symmetry of 3. On this basis the pattern could arise from either [13]

(i) the $\langle 1\,1\,1\rangle$ zone axis of a cubic structure with a larger unit cell than that for bcc α-AlFeSi;

(ii) the $\langle 0\,0\,1\rangle$ zone axis of a hexagonal crystal; or

(iii) the $\langle 0\,0\,1\rangle$ zone axis of a rhombohedral crystal.

Which of these possible structures is the correct one can

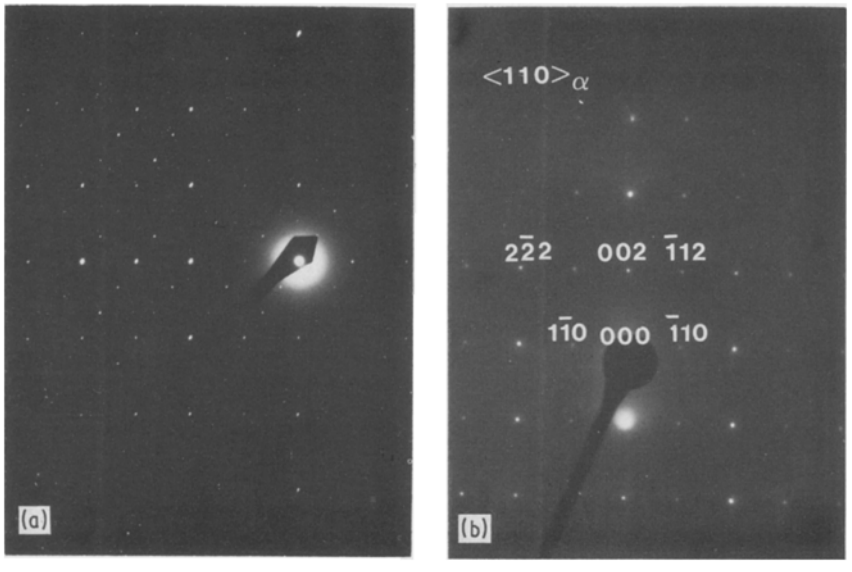

Figure 2 SAED patterns of bcc α-AlFeSi with a $\langle 1\,1\,0\rangle$ zone axis. (a) Alloys A, B and C. Extra reflections due to a superlattice are visible at 1/3 ($\bar{1}\,1\,2$) and 1/3 ($2\,\bar{2}\,2$). (b) Die-cast AlSiCu alloy. No extra reflections are visible.

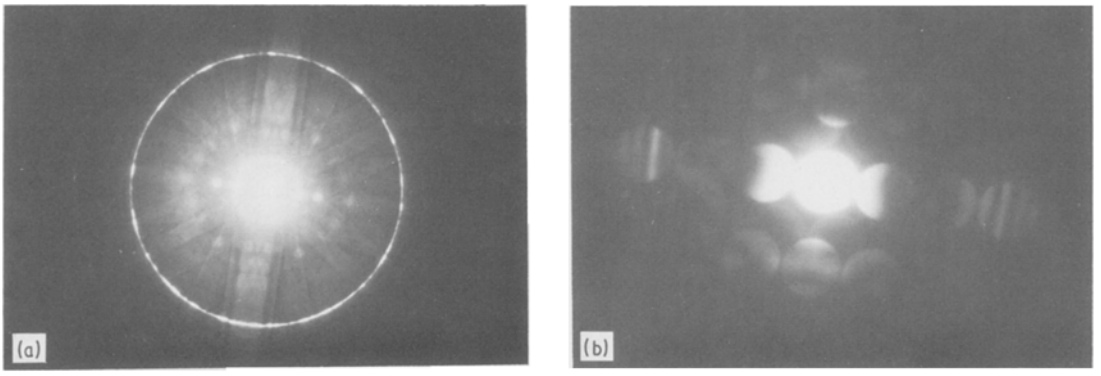

Figure 3 CBED pattern of long-range ordered α-AlFeSi with a ⟨1 1 0⟩ zone axis. (a) Whole pattern. (b) The zero order Laue zone.

be determined by the spacing of the reciprocal plane in the direction of the pattern zone axis. As stated previously, $d^*_{111} = 3d^*_{xyz}$ where $x\,y\,z$ are the indices of the innermost HOLZ ring. Thus the extra HOLZ rings arise from a superlattice which is three times larger in this direction than the primary b c c α-AlFeSi lattice.

For possible cubic superlattices, it was found that the lattice parameters obtained by indexing of reflections in CBED patterns differed to that given by the measurement of the radii of the HOLZ rings. Similarly the lattice parameters obtained from SAED patterns, when assuming a hexagonal superlattice, did not agree with that given by the radii of the HOLZ rings. Thus the superlattice can be neither cubic nor hexagonal. If a rhombohedral superlattice is assumed then it is found that indexed SAED patterns give consistent results when compared to the radii of the HOLZ rings. The lattice parameters so obtained are: $a_{sup} = 3.076\,nm$ and $c_{sup} = 3.263\,nm$. The CBED pattern in Fig. 4a corresponds to $\langle 0\,0\,1\rangle_{sup}$ for the rhombohedral superlattice. Similarly, the SAED pattern in Fig. 2a and the CBED pattern in Fig. 3 correspond to $\langle 2\,1\,0\rangle_{sup}$.

Comparison of the $\pm G$ symmetry of HOLZ reflections in CBED patterns shows that the symmetry is 2_R [13]. This implies that the superstructure maintains an inversion centre for the primary b c c α-AlFeSi structure and hence the superstructure is centrosymmetric. The point group of the superlattice is therefore $\bar{3}$ [13].

4. Structure model considerations

Ordered structures of vacancies in Al–Ni, Al–Ni–Fe and Al–Cu–Ni intermetallic compounds have been studied extensively [14–18]. In the present case it can be noted that the $\langle 1\,1\,0\rangle_{bcc}$ SAED pattern in Fig. 2a is similar to the ⟨1 1 0⟩ pattern from the τ_3 ordered structure of Al_6NiCu_3. The τ_3 structure is a rhombohedral ordering of nickel atom vacancies [16]. Thus, while the primary structure of b c c α-AlFeSi is more complex than that for Al_6NiCu_3, it seems possible that the transition metal elements, iron and nickel, behave in a similar way as in the electron phases [18]. Because iron and nickel have similar electron structures, it is hypothesized that the superlattice in b c c α-AlFeSi is due to an ordering of iron atom vacancies in a similar way to that of nickel atom vacancies in Al_6NiCu_3 or $AlNi_{1-x}$ phases [14] and that a structural model can be constructed in a similar way.

Ordering is usually accompanied by a decrease in symmetry in such a way that the point group of the ordered structure is a subgroup of the point group of the disordered structure. As the same is true for lattice translation symmetry [17], the space group of the ordered structure should then be $R\bar{3}$.

Transformations of coordinates from the disordered to the ordered structure can be obtained from Fig. 4a because

$$\begin{bmatrix} 1 & \bar{2} & 0 \\ 1 & 1 & 0 \\ 0 & 0 & 3 \end{bmatrix} \begin{bmatrix} a^*_{sup} \\ b^*_{sup} \\ c^*_{sup} \end{bmatrix} = 1/3 \begin{bmatrix} 1 & 1 & 2 \\ 2 & 1 & 1 \\ 2 & 2 & 2 \end{bmatrix} \begin{bmatrix} a^* \\ b^* \\ c^* \end{bmatrix} \quad (4)$$

where a^*, b^*, c^*, and a^*_{sup}, b^*_{sup}, c^*_{sup} are basis vectors in reciprocal space for disordered and ordered

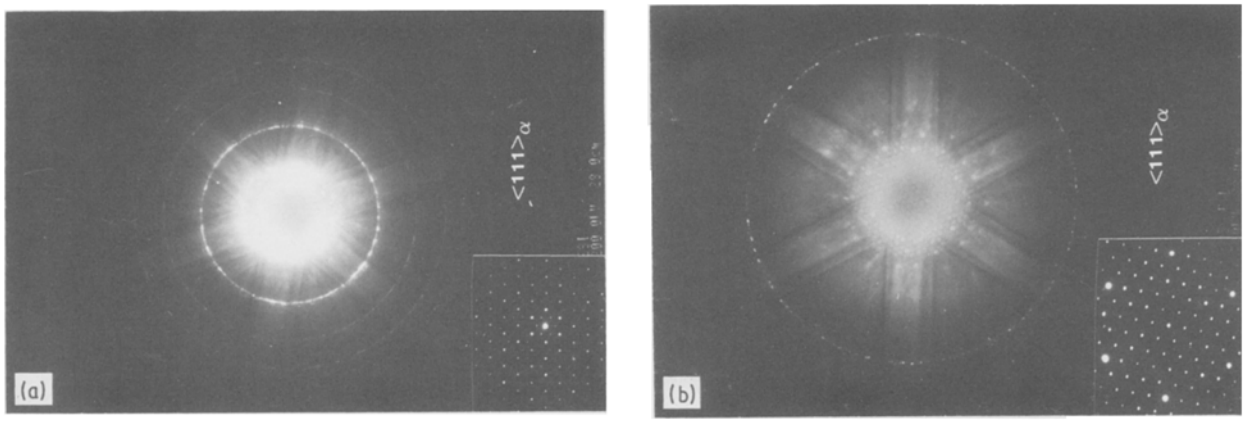

Figure 4 CBED patterns of α-AlFeSi with a ⟨1 1 1⟩ zone axis. Both patterns have the same camera length. (a) Long-range ordered α-AlFeSi with extra HOLZ rings due to the presence of a superlattice. (b) Disordered α-AlCuSi. The HOLZ ring is due to the b c c lattice.

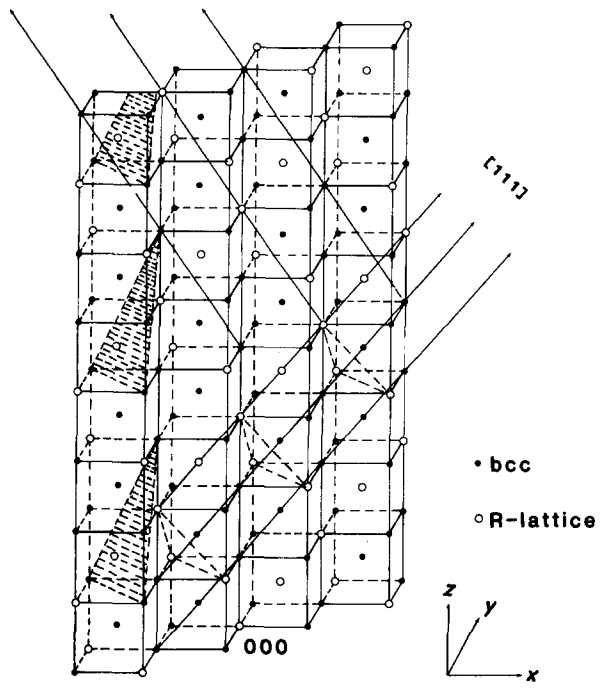

Figure 5 Structural model of the superlattice in α-AlFeSi based upon the long-range ordering of iron vacancies.

structures, respectively. Then

$$\begin{bmatrix} a_{sup} \\ b_{sup} \\ c_{sup} \end{bmatrix} = 1/2 \begin{bmatrix} 2 & \bar{4} & 2 \\ 2 & 2 & \bar{4} \\ 3 & 3 & 3 \end{bmatrix} \begin{bmatrix} a \\ b \\ c \end{bmatrix} \quad (5)$$

and

$$\begin{bmatrix} a \\ b \\ c \end{bmatrix} = 1/9 \begin{bmatrix} 3 & 3 & 2 \\ \bar{3} & 0 & 2 \\ 0 & \bar{3} & 2 \end{bmatrix} \begin{bmatrix} a_{sup} \\ b_{sup} \\ c_{sup} \end{bmatrix} \quad (6)$$

where a, b, c and a_{sup}, b_{sup}, c_{sup} are basis vectors in crystal space for disordered and ordered structures, respectively [19].

Here, the three-fold roto-inversion axis, $\bar{3}$, is along the [1 1 1] direction of the disordered structure. The coordinates of each of 24 Fe atoms from the disordered structure can now be transformed to the ordered structure. If an Fe vacancy is inserted into the disordered structure then there must be 6 Fe vacancies which are related by the three-fold roto-inversion axis along [0 0 1] of the ordered structure. In order to calculate the composition of the ordered structure the volume of the superlattice unit cell needs to be known.

TABLE II Compositions (at %) of bcc α-AlFeSi

	Fe	Al + Si
Predicted composition for the disordered stoichiometric condition	17.4	82.6
Predicted composition from the model for the iron vacancy superlattice	14.9	85.1
Experimental composition of long-range ordered precipitates*	13.9 ± 0.8	86.1 ± 1.0

*Indicated errors are standard deviations from a large number of measurements.

Only the point group was considered when it was argued that 6 Fe vacancies are related by the three-fold roto-inversion axis along [0 0 1] of the ordered structure and no translation symmetry was involved. Therefore the cubic cell has to be considered as a primitive one and there should be 9 × 6 = 54 Fe vacancies in the primitive unit cell of the superstructure. For the unit cell of the primary bcc lattice the number of Fe vacancies should be:

$$54 \frac{V}{V_{sup}} = 54 \times 1/9 \times 2/3 = 4 \quad (7)$$

where the factors 2 and 3 are the multiplicities for the bcc lattice and R-lattice, respectively. A lattice model for the ordered iron vacancy superstructure is shown in Fig. 5. In this model the composition of the bcc unit cell should be 114 (Al + Si) atoms and 20 Fe atoms. When stoichiometric, this unit cell should contain 24 Fe atoms [1].

The point group of the primary bcc structure is $m\bar{3}$ of order 24 and the point group of the ordered superstructure is $\bar{3}$ of order 6. Group theory states that the variants of the ordered iron vacancy superlattice will then be of the order of its related factor group [20], i.e.

$$24/6 = 4 \quad (8)$$

Thus the ordered structures in all four $\langle 1\,1\,1 \rangle_{bcc}$ directions are crystallographically equivalent and are related by the variant generating set (in this case the group) V.G., i.e.

$$\text{V.G.} = (1, m, 2) \quad (9)$$

where 1, m and 2 are the identity, mirror and two-fold rotation axis, respectively.

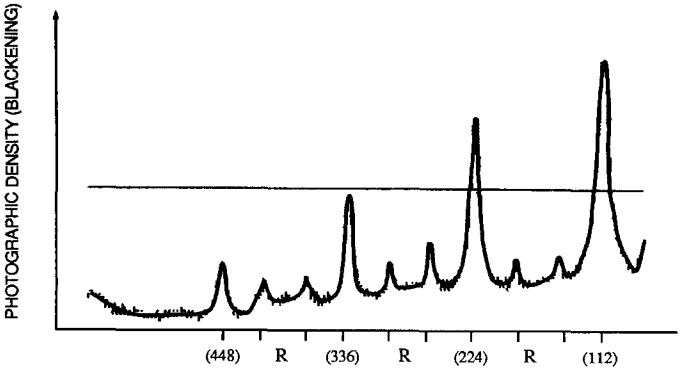

Figure 6 Photographic density measurements made on the negative of an SAED pattern. The indices of the primary reflections are indicated.

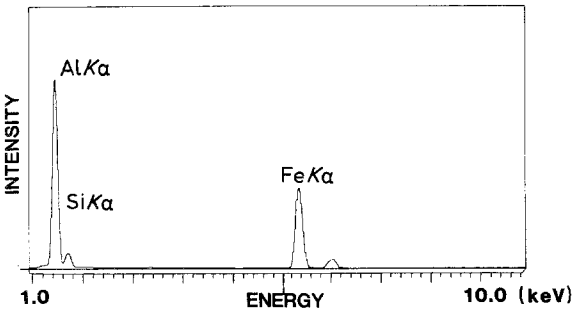

Figure 7 A typical EDX spectrum obtained from long-range ordered α-AlFeSi.

5. Comparison of the model with experimental data

5.1. Positions of superlattice reflections

From the model for the superlattice shown in Fig. 5 it can be seen that the lattice points containing ordered vacancies introduce a three times larger periodicity in both $\langle 1\,1\,1\rangle_{bcc}$ and $\langle 1\,1\,2\rangle_{bcc}$ directions and this periodicity overlaps with the primary b c c lattice. This gives rise to reciprocal lattice vectors of $1/3\ \{1\,1\,1\}_{bcc}$ and $1/3\ \{1\,1\,2\}_{bcc}$. Thus the positions of extra reflections in Fig. 2a and other SAEDs can be explained by the model.

5.2. Relative intensities of superlattice and primary reflections

Predicted relative intensities of superlattice reflections compared to that of primary reflections can be calculated from the model. For this calculation an approximation was made and only structure factors were considered. The predicted relative intensities are:

$$I_{sup}/I_{prim} = 10\% \qquad (10)$$

where I_{sup} and I_{prim} are the intensities of superlattice and primary b c c reflections, respectively. Measurements of photographic intensities on negatives of SAED patterns (Fig. 6) gave

$$I_{sup}/I_{prim} \approx 11\% \qquad (11)$$

which must be considered as very good agreement.

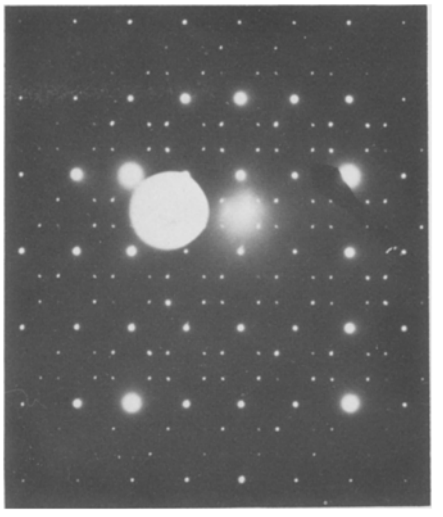

Figure 8 SAED pattern ($\langle 1\,1\,0\rangle$ zone axis) with extra reflections from four variants of the ordered structure. This pattern should be compared to that in Fig. 2a.

5.3. Composition of ordered α-AlFeSi

A typical EDX spectrum from ordered α-AlFeSi is shown in Fig. 7. Quantification of several spectra of this type gave the chemical analyses shown in Table II. Here it can be seen that the measured composition is very close to that predicted by the model and substantially different to that expected for stoichiometric b c c α-AlFeSi.

5.4. Variants of the ordered structure

The SAED pattern in Fig. 8 shows the four variants of the ordered structure as predicted by the model, i.e. if the operation of 1, m, 2 (i.e. group 2/m) is made on the SAED pattern in Fig. 2a, then a pattern of the type shown in Fig. 8 is obtained.

5.5. High-resolution imaging of the ordered lattice

It may be thought that the extra reflections in electron diffraction can arise from the presence of microtwinning. However, the high-resolution lattice image of the ordered structure shown in Fig. 9 shows clearly

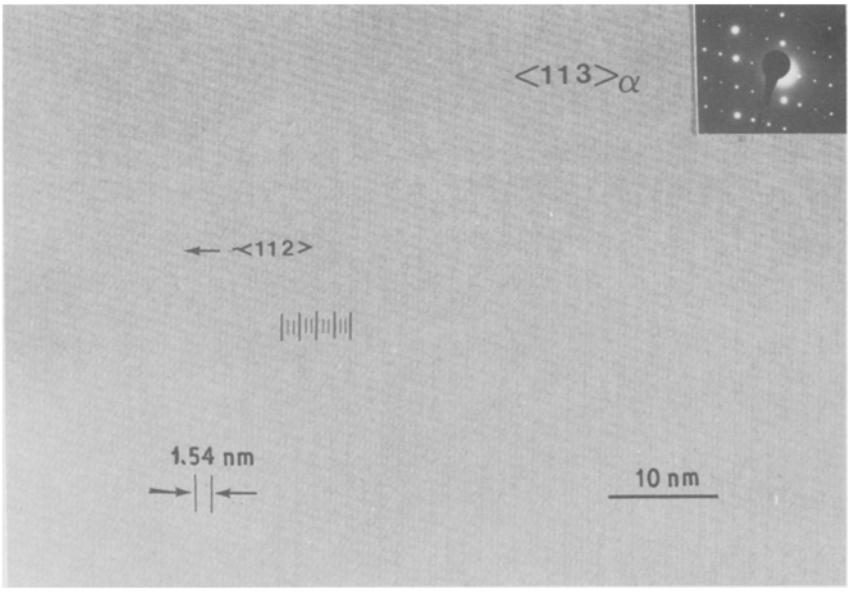

Figure 9 High-resolution lattice image of the long-range ordered α-AlFeSi structure. Dark fringes correspond to the lattice. Note that every third (1 1 2) fringe is darker.

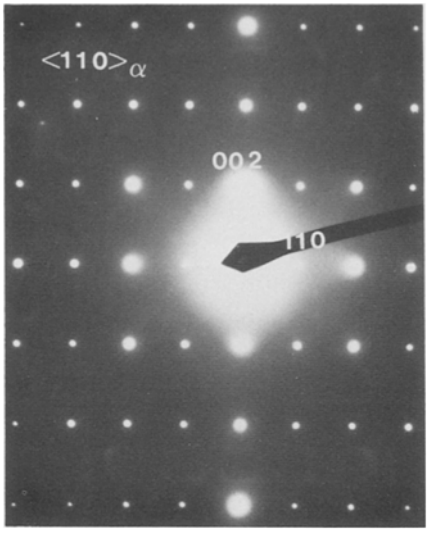

Figure 10 Diffuse electron scattering in a ⟨1 1 0⟩ zone axis SAED pattern of α-AlFeSi indicating the presence of short-range order. This pattern was obtained after irradiating a previously long-range ordered precipitate with an incident beam of 200 kV electrons for ~ 10 min. Compare with Fig. 2a.

that micro-twinning does not occur in this structure. In this image there is a clear periodicity in strong contrast (dark) from every third $(1\,1\,2)_{bcc}$ lattice plane. This periodicity is expected from the model shown in Fig. 5.

6. Short-range ordering

Irradiation of ordered α-AlFeSi with a condensed beam of electrons at 200 kV in the electron microscope for 10 min, results in loss of the extra reflections from SAED patterns and retention of weak patterns of diffuse scattered electrons as shown in Fig. 10. This is interpreted as being due to a loss of long-range ordering with a retention of some short-range ordering. The long-range ordering effect is highly sensitive to the exact positions of iron atom vacancies and, as soon as these vacancies move an interatomic distance, long-range order is lost.

7. Conclusions

1. Extra reflections in electron diffraction patterns obtained from bcc α-AlFeSi are due to long-range ordering of iron vacancies in the structure.

2. The superstructure is rhombohedral with space group $R\bar{3}$ and lattice parameter $a_{sup} = 3.076$ nm, $c_{sup} = 3.263$ nm.

3. A model for this superstructure has been presented and it has been shown that this model agrees with:

(i) the positions of superlattice reflections;
(ii) the relative intensities of superlattice and primary reflections;
(iii) the composition of the ordered phase;
(iv) the number of variants of the ordered structure;
(v) high resolution images of the crystal lattice.

4. Irradiation of the long-range ordered structure with electrons results in eventual loss of long-range ordering but retention of some short-range order.

Acknowledgements

The assistance of K.-G. Strid in measuring photographic intensities on diffraction patterns is gratefully acknowledged as is the financial support of the Swedish Board for Technical Development.

References

1. M. COOPER, *Acta Crystallogr.* **8** (1967) 1106.
2. L. F. MONDOLFO, "Aluminium Alloys: Structure and Properties" (Butterworths, London, 1976) pp. 282–91, 534–7.
3. D. MUNSON, *J. Inst. Met.* **95** (1967) 217.
4. P. LIU, T. THORVALDSSON and G. L. DUNLOP, *Mater. Sci. Technol* **2** (1986) 1009.
5. T. TURMEZEY, in Proceedings 8th European Congress on Electron Microscopy, Budapest, August (1984), edited by Á. Csanády, P. Röhlich and D. Szabó (the Programme Committee for the Congress) Vol. 1, pp. 741–2.
6. A. L. DONS, *Z. Metallkde* **15** (1984) 170.
7. P. LIU and G. L. DUNLOP, in Proceedings of International Conference on Aluminium Alloys, "Aluminium Alloys: Their Physical and Mechanical Properties", edited by E. A. Starke Jr and T. H. Sanders Jr. (EMAS, London, 1986) Vol. 1, pp 3–16.
8. G. CLIFF and G. W. LORIMER, *J. Microsc.* **103** (1975) 203.
9. P. M. KELLY, A. JOSTSONS, R. G. BLAKE and J. G. NAPIER, *Phys. Status Solidi (a)* **31** (1975) 771.
10. J. W. STEEDS, in "Quantitative Electron Microscopy", edited by J. N. Chapman and A. J. Craven (Scottish University Summer School in Physics, Edinburgh, 1984) pp. 49–96.
11. P. LIU and G. L. DUNLOP, in Proceedings 11th International Congress on Electron Microscopy, 1986 Kyoto, edited by T. Imura, S. Maruse and T. Suzuki (The Japanese Society of Electron Microscopy, Tokyo, 1986) Vol. 1, pp. 703–4.
12. P. LIU, Ph.D thesis, Chalmers University of Technology, 1986.
13. B. F. BUXTON, J. A. EADES, J. W. STEEDS and G. M. RACKHAM, *Phil. Trans. R. Soc.* **A281** (1976) 171.
14. H. LIPSON and A. TAYLOR, *Proc. R. Soc.* **A173** (1939) 232.
15. S. S. LU and T. CHANG, *Acta Sinica* **XIII** (2) (1957) 150.
16. R. DE RIDDER, G. VAN TENDELOO and S. AMELINCKX, *Phys. Status Solidi (a)* **43** (1977) 133.
17. M. VAN SENDE, R. DE RIDDER, J. VAN LANDUYT and S. AMELINCKX, *ibid.* **50** (1978) 587.
18. T. B. MASSALSKI, in "Physical Metallurgy", Part I, edited by R. W. Cahn and P. Haasen (North-Holland Physics, Amsterdam, 1983) pp. 178–218.
19. T. HAHN (ed.), "International Tables for Crystallography", A, (Reidel, Boston, 1983).
20. G. VAN TENDELOO and S. AMELINCKX, *Acta Crystallogr,* **A30** (1974) 431.

Received 12 June
and accepted 27 August 1987